International Journal of Heat and Mass Transfer 52 (2009) 1374–1384

Contents lists available at ScienceDirect

International Journal of Heat and Mass Transfer

journal homepage: www.elsevier.com/locate/ijhmt

Thermal characterisation of embedded heat spreading layers in rectangular heat-generating electronic modules

J. Dirker, J.P. Meyer *

Department of Mechanical and Aeronautical Engineering, University of Pretoria, Pretoria 0002, South Africa

ARTICLE INFO

Article history:
Received 17 January 2006
Available online 22 October 2008

Keywords:
Embedded
Conductive
Heat spreading layers
Electronics
Power electronics

ABSTRACT

The cooling performance of heat spreading layers, consisting of materials that have relatively high thermal conductivity embedded into heat-generating mediums, presents itself as a viable method of reducing peak operating temperatures in, for instance, integrated power electronic applications. In this paper the boundary condition associated with single-directional heat extraction during the cooling of a generalised rectangular, three-dimensional heat-generating volume is considered numerically. Numerically based correlations are given from which the cooling performance of a layered structure can be calculated. These correlations are based on data for large ranges in geometric dimensions, thermal conductivities, fraction of volume used for cooling purposes, and high interfacial resistance values.

1. Introduction

When considering for instance the shift towards the modular integration of power electronics, it is evident that the development of more effective cooling methods to reduce peak operating temperatures has become crucial. Due to the relatively low thermal conductivities associated with the outer material layers of these integrated power electronic modules, surface cooling on its own is no longer sufficient to keep core temperatures within allowed ranges, resulting in the constituting materials themselves acting as major thermal barriers. Associated with the high external thermal impedance, a restriction is placed on the maximum achievable power densities within such electronic modules [1,2].

Internal solid-state heat transfer augmentation of heat-generating volumes, as is found in electronic components, may be a useful tool to allow for smaller, more powerful components. This can be achieved by reducing the thermal resistance between hot internal regions and cooled surface regions. One such approach entails the creation of strategic thermal conductive pathways to aid the flow of heat towards regions serviced by relatively higher levels of cooling. This effectively should result in more uniform heat distribution within the composite volumes caused by an increase in the equivalent thermal conductivity of the structure.

Conductive cooling, being a passive cooling scheme not dependent on other support systems, exhibits some extent of reliability and volumetric advantages. Even though the temperature drop over long distances associated with conductive heat transfer may be orders higher than the temperature drops associated with, for instance, convection or evaporation, its reliability aspect justifies in-depth investigations into cooling methods using this heat transfer mode.

More recently, conductive cooling of heat-generating volumes has been approached as a volume-to-point or area-to-point heat transfer problem [3–5]. For this purpose, "thermal tree" theories were developed to describe the distribution of low thermal resistant paths and to optimise heat transfer to certain points.

Even though thermal tree schemes present optimised heat transfer performance, they more often than not require complex geometric lay-outs, which at small dimensional scales can lead to high manufacturing costs. In passive power electronic modules, which typically have inductive, capacitive and transformative functions, restrictions imposed by the electromagnetic fields dictate that only parallel-running internal embedded solid geometries can be considered. Such lay-outs, when placed in-line with magnetic field lines reduce the interference a cooling insert may have on magnetic field distribution. Three-dimensional thermal path networks are thus not suitable for such applications and much simpler pathways will need to be considered.

In a previous investigation [6], the thermal performance of a grid of discrete parallel-running high thermally conductive rectangular solid inserts, aiding the flow of heat in a single-direction was studied and geometrically optimised in terms of fixed volume use. At the dimensional scale of interest in electronics cooling, it was found that for such a configuration, the geometric shape of embedded cooling inserts has a diminishing influence on thermal performance as dimensions are scaled down [7]. With this in mind, it may be appreciated that from an economic and manufacturing

* Corresponding author. Tel.: +27 12 420 2590; fax: +27 12 362 5124.
E-mail address: jmeyer@up.ac.za (J.P. Meyer).

0017-9310/$ - see front matter © 2008 Elsevier Ltd. All rights reserved.
doi:10.1016/j.ijheatmasstransfer.2007.10.045

Nomenclature

a_{ZY} [–] y–z view aspect ratio of rectangular region between the mid-plane surfaces of two adjacent heat spreading layers
C_{GTP} [m^3K/W] coefficient dependent on geometric, thermal and material property values
e [–] exponent power of α to calculate $E_{\%,eff}$
$E_{\%,eff}$ [%] effective thermal performance increase (or allowable volumetric heat generation density increase for a given peak temperature)
k [W/mK] thermal conductivity
$\dot{q}'''$ [W/m^3] volumetric heat generation density
R [m^2K/W] interfacial thermal resistance
T [K] temperature
x [m] Cartesian axis direction
y [m] Cartesian axis direction
z [m] Cartesian axis direction

Special characters
α [–] volume fraction ratio
$\mathscr{A}$ [m] half x-directional dimension of heat-generating solid
$\mathscr{B}$ [m] half centre-to-centre offset distance between heat spreading layers in the y direction
ℓ [m] half y-directional width of heat spreading layer
γ [–] ratio between thermal conductivities of heat spreading layer and the heat-generating solid
ε [–] relative $E_{\%,eff}$ value in terms of maximum $E_{\%,eff}$
θ [–] coefficient for calculating $E_{\%,eff}$
ζ [–] adjustment factor for critical layer aspect ratio in terms of α and γ.
Z [m] half z-directional dimension of heat-generating solid

Subscripts
C heat spreading layer
eff volumetric effective expression
ext external: towards external heat sink
int internal: between heat spreading layers and heat-generating material
M heat-generating medium
max maximum
min minimum
0 ambient or reference temperature

Superscripts
$*$ critical layer condition (upper asymptotic thermal performance reached)

point of view continuous heat spreading layers provide a more practical embedded conductive cooling configuration than a gird of discrete parallel-running solid inserts.

In an experimental investigation a significant increase in the allowable heat generation density could be achieved with the inclusion of aluminium nitride layers into a ferrite magnetic core [8]. It has also been shown that the inclusion of cooling disks into circular electromagnets can result in higher magnetic performances [9]. Considering the cooling performances of high conductive layers is by no means a new concept. It has long been realised that the copper layering on printed circuit boards aid in the conductive cooling of such configurations [10]. Due to the complex nature of heat flow patterns in such conditions, rough estimates for equivalent planar and normal conductivity have been in common use. This however is an over simplification of the thermal conditions and will most likely lead to an underestimation of peak temperatures. Little material in the literature was found which focuses on thermal aspects of composite layered solids.

This paper focuses on thermal characterisation of uniform rectangular heat spreading layers and aims to provide information on thermal performance and its dependence on material properties, geometric sizes and shapes, as well as interfacial thermal resistance. The findings reported on here are not intended to be only relevant to a specific application but are rather intended for use to describe the general heat removal capabilities of heat spreading layers. A holistic approach is followed and wide ranges in material properties, interfacial resistance values and geometric parameters are covered.

2. Thermal modelling

Of interest to heat sink cooling is the use of one-sided and double sided cooling where heat is allowed to be removed from a component or a package in one direction or in two opposite directions. In Fig. 1a, a representation is given of a general heat-generating solid volume being cooled from two opposite sides by means of heat sinks. The dominant heat transfer has been chosen to be in the *z-direction*. The heat sinks can however be replaced by other types of "cold regions" such as solids cooled by micro channels or heat pipes. For the shown configuration as well as for cases of one-sided cooling (component only being in contact with one heat sink) heat transfer is dominant in one direction. By placing internal heat spreading layers parallel to the dominant heat transfer direction increased heat transfer from the heat-generating solid may be achieved. A cooling-layer model problem representative of such condition was defined as shown in Fig. 1b. With this model the thermal behaviour of layered structures could be investigated.

The model problem depicts a composite heat-generating solid which is constituted by alternating heat-generating and heat spreading layers in the y-direction, each of which has dimensions $2\mathscr{A}$ and $2\mathscr{Z}$ in the x- and z-directions, respectively. In the y-direction heat spreading layers are at a constant centre-to-centre offset distance of $2\mathscr{B}$, with each layer having a thickness of 2ℓ. The thermal conductivities of the heat-generating medium and heat spreading layer material are defined as k_M [W/mK] and k_C [W/mK], respectively. For investigation purposes in this paper uniform heat generation density within heat-generating layers is adopted and represented henceforth by $\dot{q}'''_M$ [W/m^3].

Uniform internal interfacial thermal resistance between the heat-generating layers and heat spreading layers is represented by R_{int} [m^2K/W], while external thermal resistance, where heat transfer to the surroundings is permitted, is represented by R_{ext} [m^2K/W]. All other external surfaces where heat transfer to the surroundings is not permitted are defined as being adiabatic.

In the thermal model representing a single-directional heat extraction case, heat transfer is only permitted towards the surroundings in the positive and negative z-directions. By recognising that the heat transfer coefficient related to free-convection is lower than the anticipated heat transfer coefficient (via an heat sink for instance) an assumption is made that relatively little heat transfer from external surfaces is present in the x and y directions. Most heat is thus expelled to the ambient via the heat sink. The surroundings of the layered structure are defined to be at a constant uniform temperature T_0 which can be used as thermal reference. With this idealised simplification it is aimed to only study the

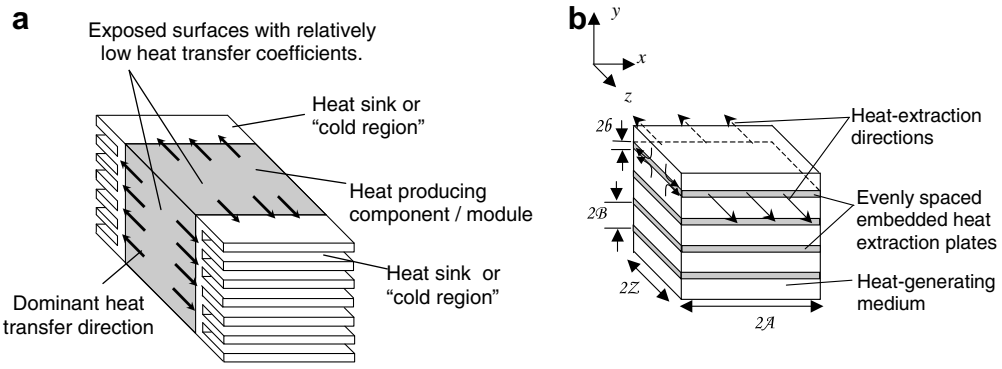

Fig. 1. Heat extraction model for conditions where heat transfer is dominant in one direction. (a) Double side cooling; (b) model problem.

influence of heat spreading layers on the internal effective thermal resistance of the composite structure. The thermal characteristics of a heat sink or other cooling devices are thus not incorporated into this study.

Due to the repetitive structure within, the symmetric nature of the model, and the fact that heat extraction to the surroundings in the *x*- and *y*-directions is assumed to be relatively small, it is possible to define a smaller representative domain, with which thermal calculations can be done. For the current single-directional boundary condition, a two-dimensional representative model is sufficient as no temperature gradients are present in the *x*-direction. A schematic diagram of the domain required by this boundary condition is given in Fig. 2. The location of the peak temperature, T_{max}, is also indicated.

The representative domain had dimensions of $\mathscr{B}$ and $\mathscr{Z}$ in the *y*- and *z*-directions. External thermal resistance was defined to be on the positive *z* face of both the heat generating and heat spreading layers. All other faces where defined to be adiabatic.

3. Numerical method

A numerical solution approach was followed as pure analytical solutions for the thermal governing equations proved to be elusive. Due to the anticipated large number of case study investigations, which were required to thermally characterise the model problems, problem specific algorithms were developed. With these algorithms the simulation processes could be automated, eliminating the time-consuming pre-processing stages required in commercial numerical software packages (more than 100,000 different geometric and material property cases where analysed in this current study).

It was the purpose of the developed algorithms to calculate the temperature fields within the domain for different input values of $\mathscr{B}, \mathscr{Z}, \ell, k_M, k_C, R_{int}, R_{ext}, T_0$, and $\dot{q}'''_M$. In order to use a numerical solution method, the domain was decomposed into hexahedral elements defined around nodal points. Uniformly spaced grid points (nodes) were defined in such a way that no grid points fell directly onto surfaces where heat transfer occurred.

A vertex centred finite volume numeric method was followed to solve for the steady state temperature field by means of a fully implicit matrix approach. The same numerical method as reported on in [11] were used in this study. With this method, the governing differential equation (as given in (1)) is discretised for rectangular three-dimensional control volumes and the variable being solved (in this case temperature) is expressed in terms of variable values of neighbouring control volumes by a single linear type equation. The governing equation used was:

$$\frac{\partial}{\partial x}\left(k\frac{\partial T}{\partial x}\right)+\frac{\partial}{\partial y}\left(k\frac{\partial T}{\partial y}\right)+\frac{\partial}{\partial y}\left(k\frac{\partial T}{\partial y}\right)+\dot{q}'''=0, \tag{1}$$

where T [K] represents temperature. The temperature discontinuity due to interfacial thermal resistance is obtained at the interface between heat-generating and heat-spreading layers by employing the following equation:

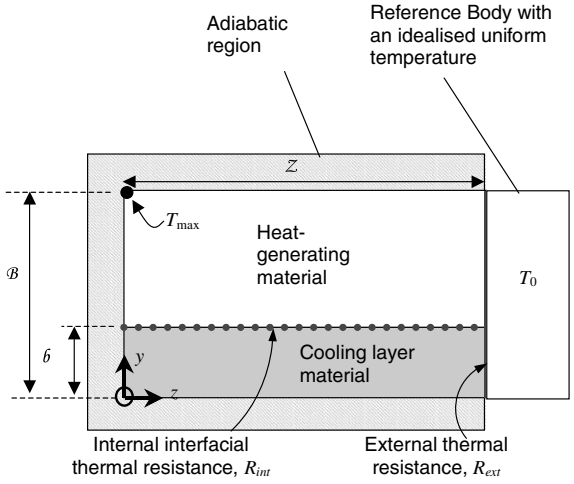

Fig. 2. Representative domain used for thermal modelling.

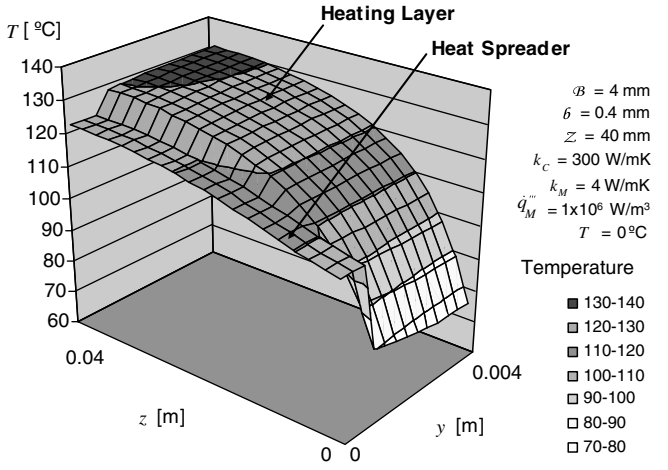

Fig. 3. Temperature distribution as obtained using the numerical model.

$$\Delta T = q''R \tag{2}$$

where ΔT [K] is the local temperature difference across the interface, q'' [W/m^2] is the local heat flux and R [m^{2}K/W] is defined as the uniform interfacial thermal resistance.

For a system with N number of grid points, N number of equations is required from which an N-by-N matrix can be constructed. LU-decomposition [12] of the constructed matrix was employed, where after back and forward substitution was used to obtain the temperature solution. A typical temperature distribution as obtained from the numerical model is shown in Fig. 3 for a chosen case.

3.1. Validation of numerical models

For the developed algorithm, it was found that mesh-independent temperature solutions are obtained when ten or more nodes are used in all Cartesian mesh directions. When the number of nodes is doubled, less than 1% difference in the calculated temperature solutions is present. For all subsequent simulation work, ten nodes were used in all relevant Cartesian directions.

The two-dimensional, single-directional numerical model was validated numerically with the use of the commercially available computational package, STAR-CD. A comparison of the temperature distributions obtained for an arbitrary case from the STAR-CD simulation result and that of the two-dimensional numerical model is shown in Fig. 4 along a nodal line in the y-direction where $z = 0$. It was found that temperature values agreed within 0.1 K of each other. Further validation was performed for a chosen geometric case using another commercial numerical package, MSC Nastran, for different interfacial thermal resistance conditions as is shown in Fig. 5. The temperature distribution in the z-direction along a line where $y = \mathscr{B}$ agreed closely for different interfacial resistance conditions. In addition to excellent numerical agreement, in a previous experimental study [8] it was found that the two-dimensional model predicted relative thermal behaviour, for a single-directional surface heat extraction case, within 5%.

4. Processing of results

With the numerical models it is possible to relate the maximum temperature rise above the heat sink (or "cold region"), $\Delta T_{\max}$ [K], to the volumetric heat generation density $\dot{q}'''_M$ [W/m^3] in terms of a thermo-geometric coefficient, C_{GTP} [m^{3}K/W] for each test case:

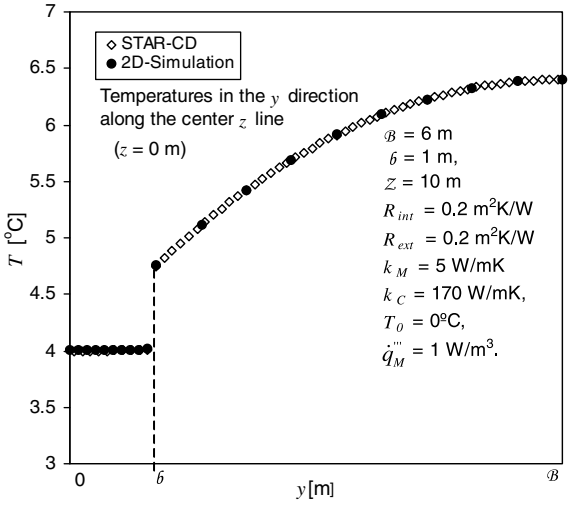

Fig. 4. Temperature distribution comparison with numerical STAR-CD results when $z = 0$ m.

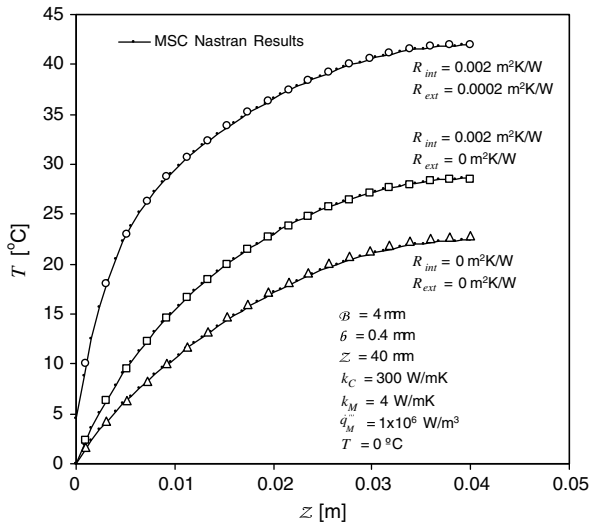

Fig. 5. Temperature distribution comparison with numerical MSC Nastran results in the z-direction when $y = \mathscr{B}$ for different interfacial resistance conditions.

$$\Delta T_{\max} = \dot{q}'''_M / C_{GTP} = T_{\max} - T_0 \tag{3}$$

Refer to Fig. 2 for the position of the maximum temperature.

The effective volumetric heat generation density increase at a fixed peak temperature, $E_{\%,effective}$ [%], can be obtained by comparing the heat generation density of a volume consisting of a uniform heat-generating medium without cooling (reference) and that of a volume which has heat spreading layers. It is defined as the percentage increase in the heat generation density in the heating layers, which the composite volume containing heat spreading layers can accommodate while maintaining the original peak temperature ($\Delta T_{\max}$ held constant):

$$E_{\%,eff} = 100(1-\alpha)\left(\left.\frac{\dot{q}'''_{M,\text{with cooling}}}{\dot{q}'''_{M,\text{no cooling}}}\right|_{\Delta T_{\max}=\text{Const}} - 1\right) \tag{4}$$

thus,

$$E_{\%,eff} = 100(1-\alpha)\left(\left.\frac{C_{GTP,\text{with cooling}}}{C_{GTP,\text{no cooling}}}\right|_{\Delta T_{\max}=\text{Const}} - 1\right) \tag{5}$$

Here α refers to the volume fraction $(\ell/\mathscr{B})$ occupied by the heat spreading layers.

5. Trends and results for cases with no thermal interfacial resistances

It was found that in cases where no internal or external thermal interfacial resistances are present, $E_{\%,eff}$ is not dependent on the absolute magnitudes of the thermal conductivities, but rather on their thermal conductivity ratio, γ [–], defined as:

$$\gamma = k_C / k_M \tag{6}$$

This occurrence might be due to the fact that thermal interfacial resistance is an area based variable while internal heat generation is volume based. Similarly, only the slenderness ratio of the two-dimensional area between the mid-plane surfaces of neighbouring heat spreading layers, a_{ZY}, influence $E_{\%,eff}$, and not the absolute magnitude of $\mathscr{B}$ and $\mathscr{Z}$. Here a_{ZY} is defined as follows:

$$a_{ZY} = \mathscr{Z}/\mathscr{B} \tag{7}$$

In Fig. 6 the impact of these two non-dimensional ratios on $E_{\%,eff}$ is demonstrated for α values of 0.1, 0.2, and 0.5 (10%, 20% and 50% of

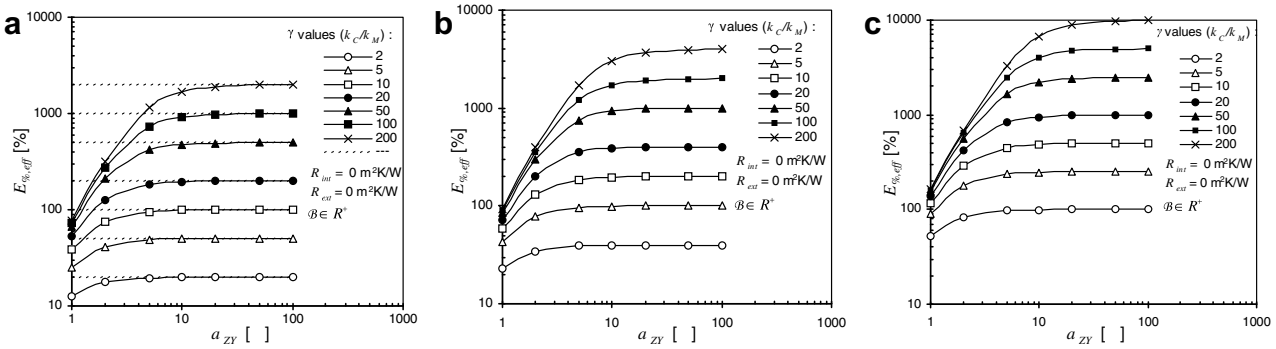

Fig. 6. Influence of a_{ZY} and γ on $E_{\%,eff}$ for no thermal interfacial resistances with different α values. (a) $\alpha = 0.1$; (b) $\alpha = 0.2$; (c) $\alpha = 0.5$.

volume used for cooling purposes). From the graphs it follows that an increase in α or γ results in higher $E_{\%,eff}$ values.

In cases with a particular α and γ, it was found that $E_{\%,eff}$ approaches an upper limit asymptote, $E_{\%,eff,\max}$, as the number of heat spreading layers is increased and their thickness reduced in proportion (thus maintaining a constant α value). This maximum value was found to be dependent only on α and γ and can be expressed as follows:

$$E_{\%,eff,\max} = 100\alpha\gamma \tag{8}$$

However, when the heat spreading layers' offset distances are excessively large, the thermal performance of a component can be deteriorated by the inclusion of heat spreading layers. The lower limit of $E_{\%,eff}$ is dependent only upon α and can be expressed as:

$$E_{\%,eff,\min} = -100\alpha \tag{9}$$

Eq. (8) gives the ultimate maximum value heat generation density can be increased by for a fixed volume fraction and relative cooling material thermal conductivity. Practically this maximum value can be approached by reducing both thermal interfacial resistances (if this value is appreciable) and the thickness of the alternating heating and heat spreading layers.

5.1. Critical layer conditions

It was found however that this equation is only valid for calculating $E_{\%,eff,\max}$ values once the critical heat spreading layer thickness and offset condition have been reached. The equation can thus not be used with confidence to compare different α and γ cases if this is not true. The slenderness or narrowness of the volume between two neighbouring heat spreading layers in the z direction can be used to describe relative layer thickness. When using the z direction, a_{ZY} can be utilised to describe critical relative conditions, which is denoted here by a^*_{ZY}. Critical conditions are assumed to have been reached once the following conditions are true (see dashed lines in Fig. 6a):

$$E_{\%,eff} \geqslant 0.99E_{\%,eff,\max} \tag{10}$$

Once this condition has been reached, no significant additional thermal performance increase is obtained by further increasing the number of heat spreading layers and reducing their thickness in proportion. The dependence of a^*_{ZY} on α and γ is demonstrated in Fig. 7 in cases where no thermal interfacial resistance is present.

From this graph it can be observed that a^*_{ZY} reaches a maximum at $\alpha = 0.5$ and that a^*_{ZY} increases as γ increases (higher a^*_{ZY} values represent conditions with thinner heat spreading layers). Practically this means that in relation, utilising heat spreading layers with higher thermal conductivities would require more, and thinner, heat spreading layers to reach maximum $E_{\%,eff}$ values, than would have been the case when using lower thermal conductivity

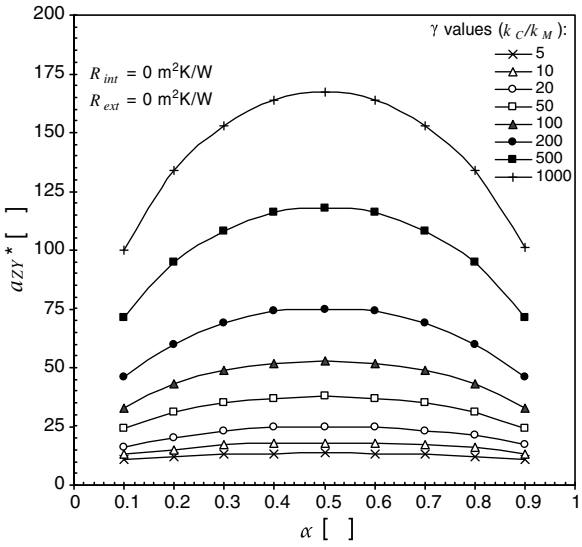

Fig. 7. Critical a_{ZY} for different α and γ values for a single-directional heat extraction boundary condition.

layers. Even though higher thermal conductivity layers exhibit higher maximum $E_{\%,eff}$ values, their ability to reach such conditions becomes very dependent upon the practical manufacturing limit of producing heat spreading layers which are thin enough. The minimum layer thickness might vary depending on the manufacturing method used and the mechanical material properties of the layers. Aspects such as thermally induced stress can also have an impact on practical layer thickness.

5.2. Non-critical layer conditions

In cases where critical layer thickness and offset distances are not present, $E_{\%,eff}$ values below that of $E_{\%,eff,\max}$ are exhibited by the system. For explanatory purposes a relative $E_{\%,eff}$ value is defined as follows:

$$\varepsilon = \frac{E_{\%,eff}}{E_{\%,eff,\max}} = \frac{E_{\%,eff}}{100\alpha\gamma} \tag{11}$$

Ratio ε is thus the proportion between the achievable $E_{\%,eff}$ for certain heat spreading layer and offset distance conditions, and the ultimate maximum $E_{\%,eff}$ value expressed by Eq. (8). $E_{\%,eff}$ can thus be expressed as follows for cases without thermal interfacial resistance:

$$E_{\%,eff} = 100\alpha\gamma\varepsilon \tag{12}$$

Fig. 8 demonstrates the dependence of ε upon α, γ and the ratio a_{ZY}/a^*_{ZY}. The ratio a_{ZY}/a^*_{ZY} serves as an indication of relative

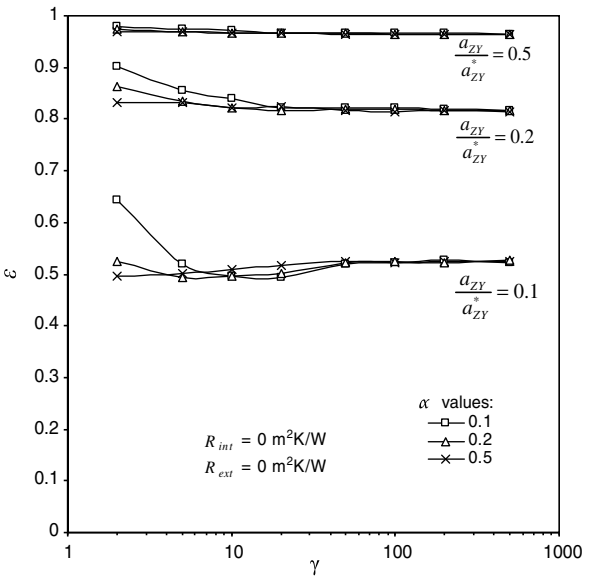

Fig. 8. ε values for cases with no thermal interfacial resistances when critical layer thickness is not reached.

layer-thickness and offset-distance conditions in terms of the critical layer thickness and offset-distance condition. From the graph it can be observed that ε is not significantly impacted on by α at γ values above 30. Also, very constant ε values are obtained for a wide range of γ values and it was found that for a_{ZY}/a^*_{ZY} ratios of 0.5, 0.2 and 0.1, ε values in the regions of 0.95, 0.8 and 0.5, respectively, are obtained. This corresponds to $E_{\%,eff}$ values of 95%, 80% and 50% of the ultimate $E_{\%,eff}$ values predicted by Eq. (8).

By combining Eq. (12) with the definitions given in Eqs. (3) and (5) the following expression for the expected peak temperature can be obtained for conditions when no interfacial thermal resistance is present, internally or externally:

$$T_{\max} \approx T_0 + \frac{(1-\alpha)Z^2}{2k_M(1+\alpha\gamma\varepsilon-\alpha)}\dot{q}'''_M \tag{13}$$

Here $C_{GTP,\text{no cooling}} = \frac{2k_M}{Z^2}$ as can be obtained by considering a one-dimensional temperature field in the dominant heat transfer direction towards the heat sinks. With the ε values contained in Fig. 8 Eq. (13) can be used to determine the expected peak temperature in a composite layered structure for a large range in geometric and material property values applicable to a single-directional heat-extraction case. The accuracy of this estimation is determined by the accuracy of ε.

6. Some trends for cases with thermal interfacial resistances

As demonstrated in Fig. 9 as an example case, the presence of thermal interfacial resistance, internally, R_{int}, and externally, R_{ex}, can dramatically increase the maximum peak temperature within a heat-generating solid. Thus, the presence of thermal interfacial resistance impacts negatively on the thermal performance of an embedded heat spreading layer scheme.

From a previous investigation [8] thermal interfacial resistance between ceramics (a suitable heat spreading material type to use in the presence of magnetic fields) and metals were found to be in the order of 0.001 and 0.0001 m²K/W when being held together via mechanical means. The use of silver loaded adhesives also exhibited similarly sized interfacial thermal resistances. In interest of an holistic approach the range in thermal interfacial resistance reported on in this paper was extended to include values as great as 0.1 m²K/W (thermal interfacial resistances of greater than 0.001 m²K/W may prove not to be practical at small or thinly spaced layers).

When thermal interfacial resistances are present the simplifications obtained by the use of ratios only, to demonstrate the impact of thermal conductivities via γ and geometrical shapes via a_{ZY}, are no longer adequate to describe $E_{\%,eff}$ values. When thermal interfacial resistance is present, not only is the shape of the heat-generating solid between two neighbouring heat spreading layers of importance, but also its physical size. Likewise, the physical magnitude of thermal conductivities becomes important, and not just the ratio between them.

The above-mentioned issues significantly increase the complexity of describing thermal performance levels for different geometric shapes, thermal conductivity and interfacial resistance values. Unlike before, single data-lines can no longer be used to describe a set of related cases. Instead, each combination of geometric aspect ratio(s), thermal conductivity sets, and thermal interfacial resistance values now requires separate trend lines.

6.1. Critical layer conditions

As before, it was found that the ultimate maximum thermal performance, $E_{\%,eff,\max}$, is still dependent upon α, γ, but now requires additional parameters as expressed below:

$$E_{\%,eff,\max} = 100\alpha^e\theta\gamma. \tag{14}$$

Here e and θ are parameters that are dependent upon k_C, k_M, R_{int}, R_{ext} and $\mathscr{Z}$. The format of this equation was derived from numerical results and was found to describe changes in $E_{\%,eff,\max}$ adequately. In conditions when critical heat spreading layer thickness and offset conditions have been reached, it was found that the internal interfacial resistance value has little impact on $E_{\%,effective}$. This might be due to the thermal resistance associated with longitudinal heat conduction in the thin-layered heat-generating medium becoming dominant due to the reduced cross-sectional area of each layer. The impact of thermal conductivity, external thermal interfacial resistance and $\mathscr{Z}$ can be described by using a powerful non-dimensional number, $\mathscr{Z}/k_M R_{ext}$. The values of θ and e are given in Figs. 10 and 11, respectively, in terms of γ and $\mathscr{Z}/k_M R_{ext}$. The values of e and θ were obtained by doing data fits on numerical data for different $\mathscr{Z}/k_M R_{ext}$ values over a range covering nine α values from 0.1 to

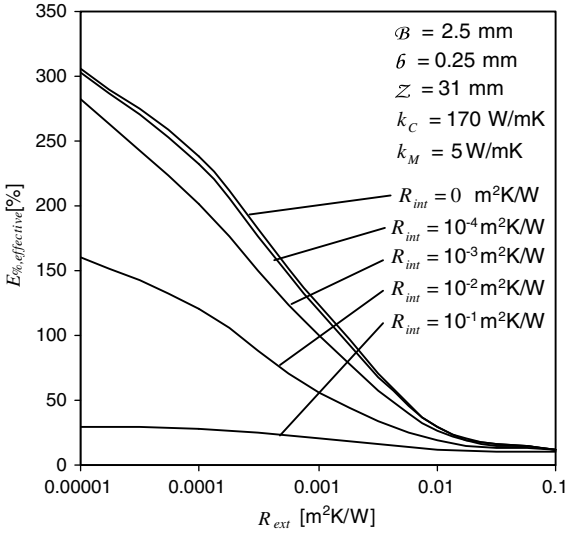

Fig. 9. Impact of thermal interfacial resistance on $E_{\%,eff}$.

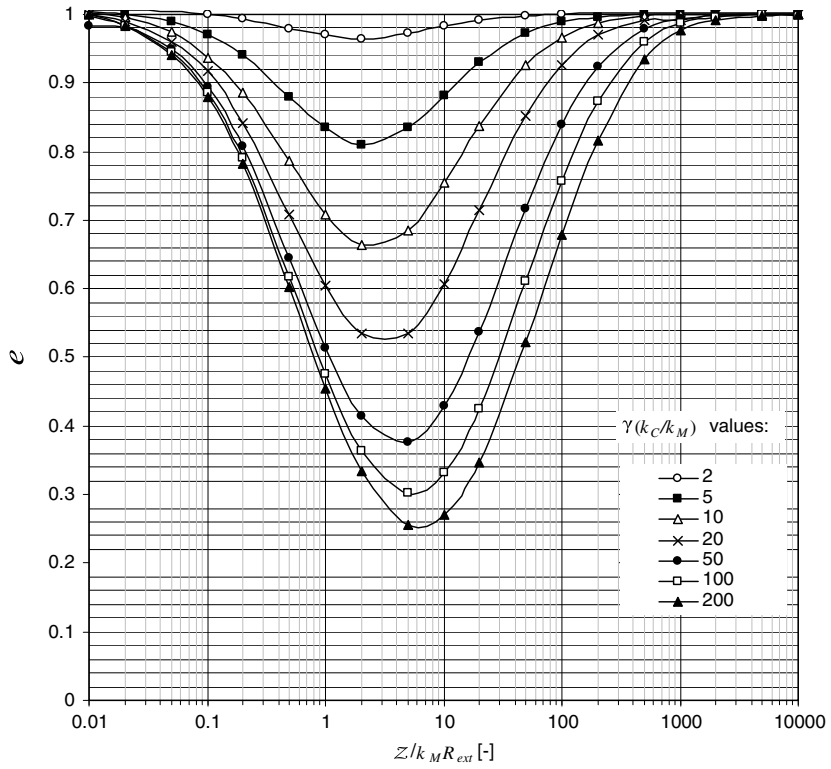

Fig. 10. Exponent of α in Eq. (14).

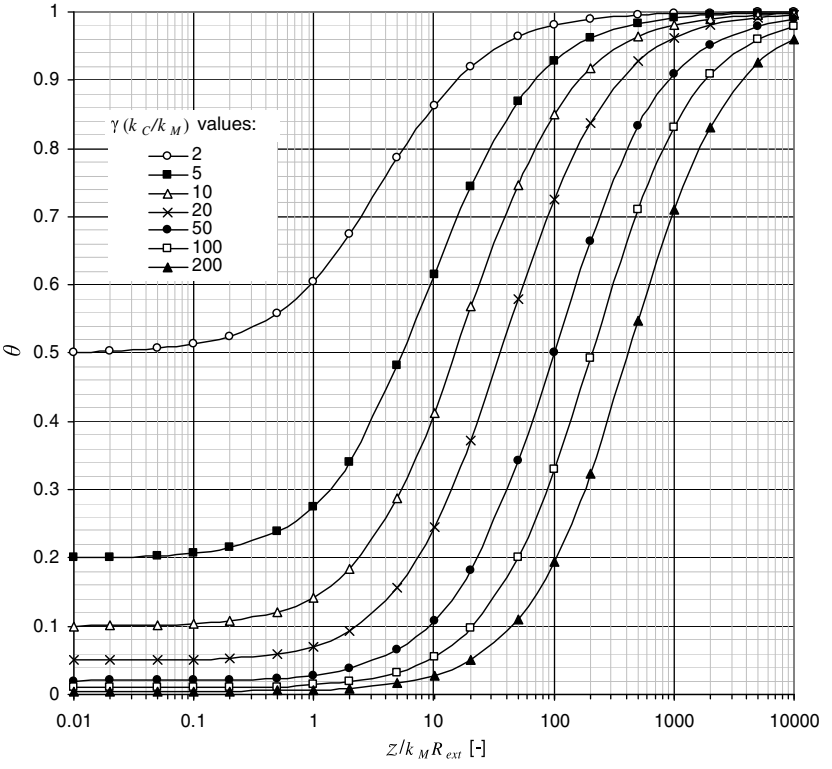

Fig. 11. Coefficient θ in Eq. (14).

0.9. The coefficient of determination (statistical term R^2) was found to be greater than 0.99 in all cases represented in these figures.

From Fig. 10 it is evident that the exponent of α, in Eq. (14) is heavily dependent on γ and $\mathscr{Z}/k_M R_{ext}$. An increase in γ results in reduced values of the exponent e. In a region of 1–10 for $\mathscr{Z}/k_M R_{ext}$, it can be seen that γ has the most dramatic influence on e. It is in this region where e reaches its lowest value. For $\mathscr{Z}/k_M R_{ext}$ values above 1000 and below 0.01, e has a value close to 1.

From Fig. 11 it can be observed that as with exponent e, the coefficient θ in Eq. (14) is also heavily dependent on γ and $\mathscr{Z}/k_M R_{ext}$. Increased γ values result in reduced θ values. As $\mathscr{Z}/k_M R_{ext}$ values become smaller they also result in lower θ values with θ reaching asymptotic limits when $\mathscr{Z}/k_M R_{ext}$ is in the region of 0.01. The asymptotic values were found to be equal to γ^{-1}.

It was further found that R_{int} values smaller than 0.1 m^2K/W, have a much lower influence on $E_{\%,eff,\max}$ than R_{ext}, but only when critical layer thickness and offset distances have been reached. It was found that $E_{\%,eff,\max}$ normally decreases by less than 1% if R_{int} was to be changed from 0 m^2K/W to 0.1 m^2K/W. It can safely be assumed that most practical cases will fall within this range. For critical conditions it appears as if the thermal resistance associated across the internal interface is still appreciably smaller than the conductive thermal resistance to the ambient via the heat-generating material.

With the data given in Figs. 10 and 11 it is possible to calculate the ultimate maximum $E_{\%,eff}$ value which can be obtained for a single-directional heat extraction case where thermal interfacial resistance is present. This calculation can be done for any z-directional dimension of the heat-generating medium, any thermal conductivity values of the heat spreading layer and heat-generating medium, and any thermal interfacial resistance value. It might be noted that the inclusion of e and θ into Eq. (14) results in lower $E_{\%,eff,\max}$ values than was the case when no thermal interfacial resistance was present and $E_{\%,eff,\max}$ could be described by Eq. (8). As expected, for low R_{ext} values the results of Eq. (14) approach that of Eq. (8) as $Z/k_M R_{ext}$ tends to infinity.

It was found that the measure of how closely a case is to critical layer conditions, a^*_{ZY}, is dependent on α, γ, the ratio between R_{int} and R_{ext}, and $Z/k_M R_{ext}$. With thermal interfacial resistance present, critical a^*_{ZY} threshold values are given in Fig. 12 for a wide range of γ and $Z/k_M R_{ext}$ values for a conditions where $R_{int} = R_{ext}$. Unlike for conditions where no interfacial thermal resistance is present, a^*_{ZY} values are no longer symmetric around $\alpha = 0.5$ as was the case in Fig. 7. Instead, it was found that for low $Z/k_M R_{ext}$ (indicating high R_{int} and R_{ext} values) higher a^*_{ZY} values are present at small α values than for larger α values as is evident by comparing graphs for $\alpha = 0.3$ and $\alpha = 0.5$ in Fig. 12. The difference in a^*_{ZY} at low $Z/k_M R_{ext}$ values when $\alpha = 0.3$ and $\alpha = 0.7$, demonstrates the unsymmetrical behaviour around $\alpha = 0.5$ when thermal interfacial resistance is present.

With the information given in Fig. 12, the maximum heat spreading layer thickness (in terms of a^*_{ZY}) can be obtained for which Eq. (14) can be used to determine $E_{\%,eff}$. The trends in these graphs are however only valid for conditions where $R_{int} = R_{ext}$. When $R_{int} \neq R_{ext}$, the given a^*_{ZY} values need to be adjusted.

It was found that when $R_{int} < R_{ext}$ ($R_{int}/R_{ext} < 1$), lower a_{ZY} values (thicker material layers) are adequate to reach critical conditions than when $R_{int} = R_{ext}$ ($R_{int}/R_{ext} = 1$), and that significantly higher a_{ZY} values (thinner material layers) are needed when $R_{int} > R_{ext}$ ($R_{int}/R_{ext} > 1$). From a practical point of view, it is expected that the external interfacial resistance would be greater than internal interfacial resistance values if the composite heat-generating component with embedded heat spreading layers was manufactured efficiently from a thermal interfacial resistance point of view. For this reason only $R_{int}/R_{ext} < 1$ is considered to a deeper extent here.

An adjustment factor, $\zeta \in (0;1]$, can be defined with which a^*_{ZY} values, as given in Fig. 12, should be changed for cases when $R_{int} \neq R_{ext}$:

$$a^*_{ZY,R_{int}/R_{ext}<1} = \zeta a^*_{ZY,R_{int}/R_{ext}=1} \tag{15}$$

It was found that the precise adjustment factor, for a particular $Z/k_M R_{ext}$ and R_{int}/R_{ext} case can be heavily dependent upon α and γ, as is demonstrated in an arbitrary case in Fig. 13 when $Z/k_M R_{ext} = 200$ and $R_{int}/R_{ext} = 0.5$. In general, it was found that smaller ζ values are obtained when either α or γ is increased. Due to the complexity of the trends involved, only general tendencies of a^*_{ZY} in terms of $Z/k_M R_{ext}$ and R_{int}/R_{ext} will be indicated here.

To conform to the rest of this paper, γ values in the range of 2–2000, α values from 0.1 to 0.9, and $Z/k_M R_{ext}$ from 10 to 10,000 are considered. Only median adjustment factors and their standard deviations for these ranges are supplied for different R_{int}/R_{ext} values. In Fig. 14 these values of ζ are given for R_{int}/R_{ext} ranging from 0.01 to 0.75. It can be seen that the adjustment factor approaches a value of 1 as $Z/k_M R_{ext}$ increases and that the greatest adjustment in a^*_{ZY} is required when $Z/k_M R_{ext}$ is small and when there is a large difference between R_{int} and R_{ext}. Standard deviation of ζ is at its largest for all R_{int}/R_{ext} values when $Z/k_M R_{ext}$ is in the range of 60–80, indicating the largest uncertainty in exact ζ in terms of α and γ.

With the information supplied in Fig. 14 it is possible to determine with relative certainty, in terms of layer thickness, when Eq. (14) can be utilised to predict the thermal performance of a heat extraction system with considerable levels of thermal interfacial resistance.

6.2. Non-critical layer conditions

When manufacturing techniques do not allow for thin enough material layer thickness, and critical conditions have not been reached, the thermal performance that could be expected will be reduced as is discussed in this section. As before, the impact of non-critical layering conditions on $E_{\%,eff}$ can be expressed by adding ε to Eq. (14) in cases where interfacial resistance is present:

$$E_{\%,eff} = 100\theta\alpha^e\gamma\varepsilon \tag{16}$$

It can be expected that ε would be less than 1. As with the first segment of this paper, it was found that ε is influenced by α, γ and a_{ZY}/a^*_{ZY}. Additionally, ε is now also dependent on $Z/k_M R_{ext}$ and R_{int}/R_{ext}.

It was found that in terms of $Z/k_M R_{ext}$, α and γ have a relatively small influence on ε. Due to this, and the complexity of individual trends, only combined generalised trends of α and γ are given here for different non-dimensional $Z/k_M R_{ext}$ and R_{int}/R_{ext} values. The ranges of α and γ considered here are, respectively, from 0.1 to 0.9 and 2 to 2000. In Fig. 15 the median ε and standard deviation of ε for these α and γ ranges are given in terms of $Z/k_M R_{ext}$ for R_{int}/R_{ext} values of 1, 0.5, 0.2 and 0.1 (each data point is based on 90 combinations of α and γ). Here a_{ZY}/a^*_{ZY} values of 0.5, 0.2, 0.1, 0.05, 0.02 and 0.01 are considered representing conditions where layer thickness are 2, 5, 10, 20, 50 and 100 times greater than the critical layer thickness described in Eq. (15).

From the graphs in Fig. 15 it can be seen that as expected, ε is reduced as layer conditions resemble critical conditions to a lesser extent (thus smaller a_{ZY}/a^*_{ZY} values are prevalent which represent higher relative layer thickness). In cases where actual relative layer thickness is twice the layer thickness required for critical conditions (represented by $a_{ZY}/a^*_{ZY} = 0.5$), ε was found to be in the region of 0.96 for all α, γ, R_{int}/R_{ext}, and $Z/k_M R_{ext}$ combinations (this is similar to the trends obtained for conditions without thermal interfacial resistance). From this, it may be expected that only about 3–4% of cooling performance will be sacrificed when doubling both heat-generating and heat spreading layer thickness. This may result in a dramatic decrease in manufacturing costs without losing a significant amount of cooling capability.

It was found that ε is more dependent upon α, γ, R_{int}/R_{ext}, and $Z/k_M R_{ext}$ as a_{ZY}/a^*_{ZY} becomes smaller. The dependence of ε on α and γ is evident by considering the higher standard deviation values of ε obtained for such cases. Due to the complexity of trends in these regions, individual dependencies on α and γ are omitted from

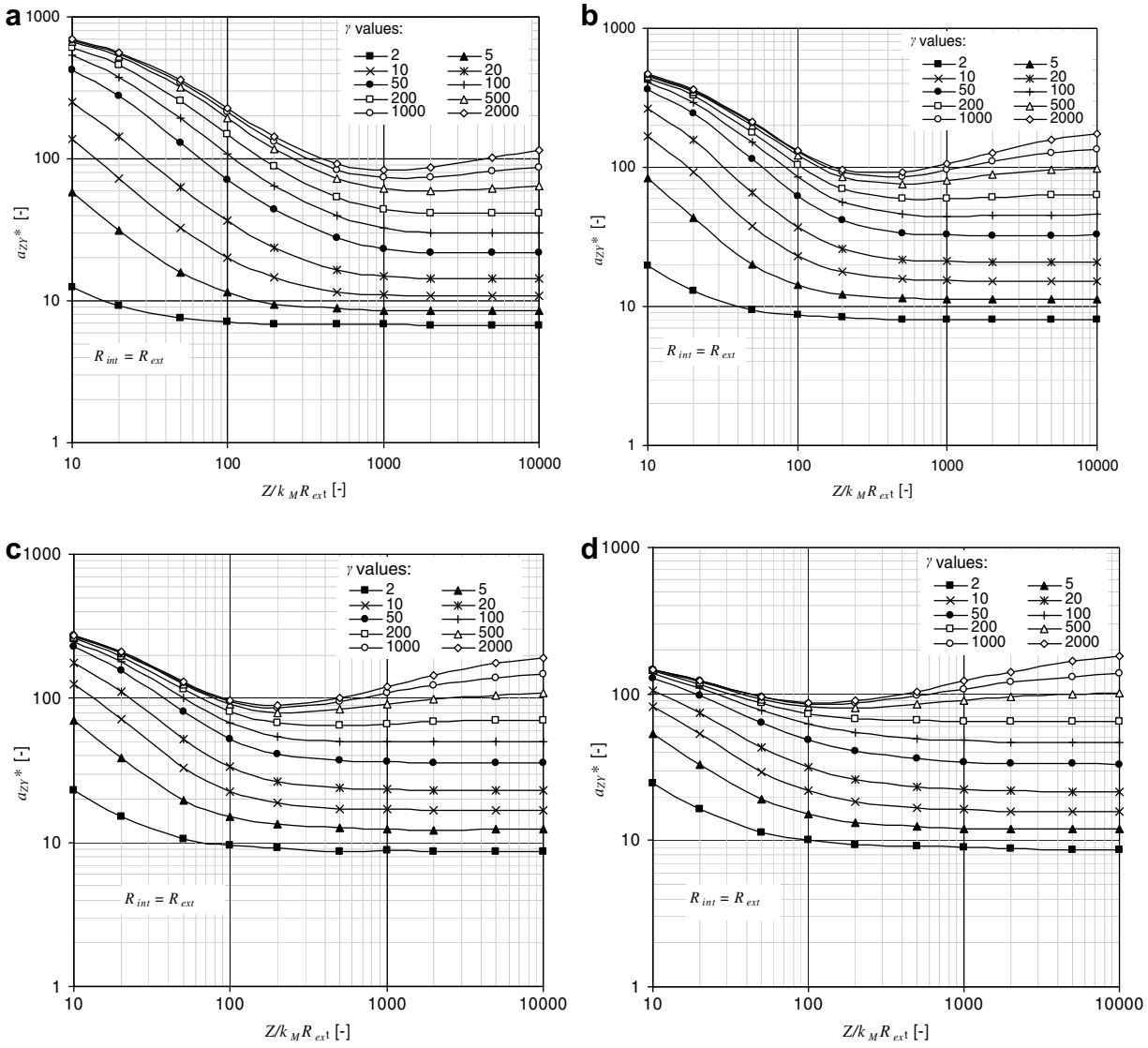

Fig. 12. Critical condition threshold for $R_{int} = R_{ext}$ for various volume fraction cases. (a) $\alpha = 0.1$; (b) $\alpha = 0.3$; (c) $\alpha = 0.5$; (d) $\alpha = 0.7$.

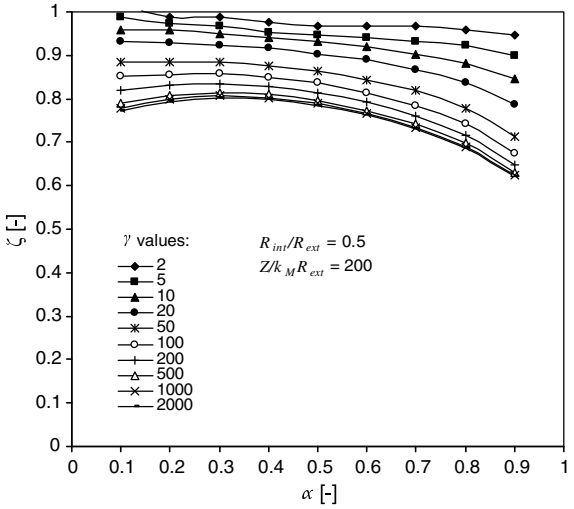

Fig. 13. Adjustment factor values for $\mathscr{Z}/k_M R_{ext} = 200$ and $R_{int}/R_{ext} = 0.5$.

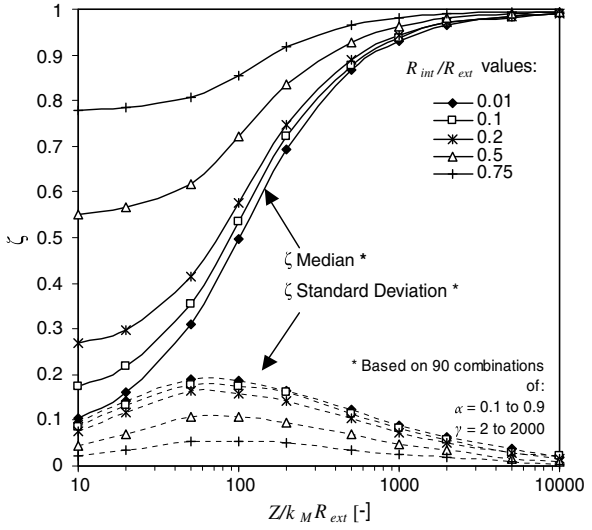

Fig. 14. Median and standard deviation values of adjustment factor, for a^*_{ZY}.

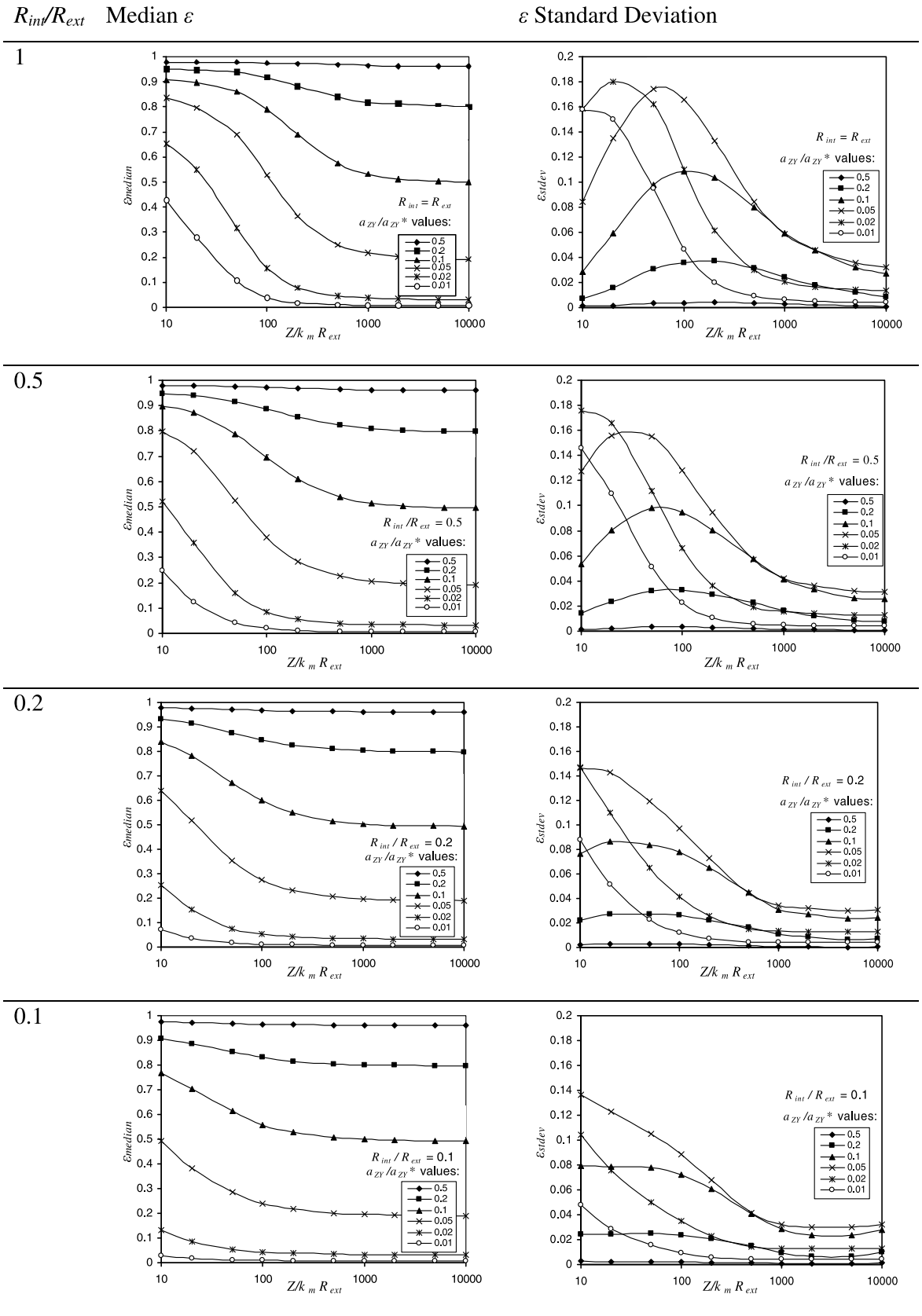

Fig. 15. Median and standard deviation ε values for various R_{int}/R_{ext} ratios and non-critical layer conditions. The results are based on 90 combinations of $\alpha = 0.1$ to $\alpha = 0.9$, and $\gamma = 2$ to $\gamma = 2000$.

this paper (refer to Fig. 16 for an arbitrary extreme case indicating the non-elementary behaviour of ε).

In terms of R_{int}/R_{ext}, it was found that ε is reduced to a greater extent when R_{int}/R_{ext} values are relatively small. Practically it

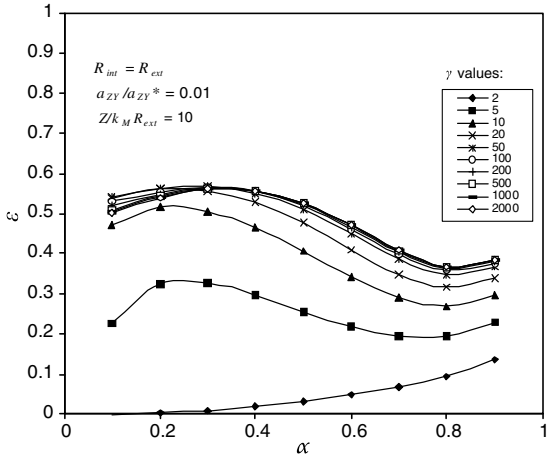

Fig. 16. Influence of α and γ on ε for an arbitrary extreme case.

may thus be expected that ε, and thus thermal performance, will be more sensitive toward layer condition when R_{int} is small in terms of R_{ext}. In general it was found that ε is less dependent on layer conditions when $Z/k_M R_{ext}$ is reduced. This represents conditions where layers are further apart in the z-direction or when higher thermal conductive materials are being used, or when external thermal resistance is relatively high.

When considering the standard deviation results, they were also found to exhibit complex trends. High standard deviation values indicate a higher uncertainty associated with using the median ε values to incorporate the impact of α and γ. It was found that the standard deviation peaked at different $Z/k_M R_{ext}$ values for different R_{int}/R_{ext} and a_{ZY}/a_{ZY}^* conditions and that in general the standard deviation was below 0.05 in cases when $Z/k_M R_{ext}$ was higher than 1000. Standard deviation values were also found to be lower as R_{int}/R_{ext} became smaller.

As before, for cases without thermal interfacial resistance, an expression can be obtained for the expected maximum peak temperature when thermal interfacial resistance is significant. This is done by combining Eq. (16) with the definitions given in Eqs. (3) and (5):

$$T_{\max} \approx T_0 + \frac{(Z^2 + 2k_M Z R_{ext})(1-\alpha)}{2k_M(\theta\alpha^e\gamma\varepsilon - \alpha + 1)}\dot{q}'''_M \tag{17}$$

Here $C_{GTP,\text{no cooling}} = \frac{2k_M}{Z^2+2k_M Z R_{ext}}$, as can be obtained by considering a one-dimensional temperature field in the dominant heat transfer direction towards the heat sinks. Thermal resistance on the interface with the heat sinks are incorporated by including R_{ext} in this expression.

By obtaining ε, e and θ values from figures such as Figs. 13, 8 and 9, respectively, Eq. (17) can be used to determine the expected peak maximum temperature in a layered composite structure for single-directional heat extraction with thermal interfacial resistance considered both internally and externally. The accuracy of this estimation is most dependent on the accuracy of ε. (The trends for e and θ had coefficients of determination of greater than 0.99.)

7. Conclusion

It has been found that the increase in allowable power densities in composite layered structures with embedded heat spreader is directly proportional to the volume fraction used for heat spreading layers, and the ratio between the thermal conductivities of the heat-generating and heat-spreading layer materials. This is true for cases where thermal interfacial resistance is negligible. However, in conditions where interfacial thermal resistance is present either internally or externally, or both, the thermal performance increase was found to be also dependent on the geometric size of the volume, the individual thermal conductivities of the material involved, as well as the individual thermal interfacial resistance values and the ratio between them. Correlations for the upper asymptotic thermal performance values were derived for conditions where the material layers become narrow and thin enough along the heat extraction direction. The published correlations for these upper limits agreed to within 1% of the numerical data. Similar correlations were also derived in cases where material layering is not in this state. Equations were derived with which the peak maximum temperature in a layered structure (subject to the specified boundary conditions) can be estimated with.

References

[1] J.D. Van Wyk, J.T. Strydom, L. Zhao, R. Chen, Review of the development of high density integrated technology for electromagnetic power passives, Proc. 2nd Intl. Conf. Integr. Power Syst. (CIPS) (2002) 25–34.
[2] F.C. Lee, J.D. Van Wyk, D. Boroyevich, T. Jahns, T.P. Chow, P. Barbosa, Modularisation and integration as a future approach to power electronic systems, Proc. 2nd Intl. Conf. Integr. Power Syst. (CIPS) (2002) 9–18.
[3] M. Almogbel, A. Bejan, Conduction trees with spacing at tips, Int. J. Heat Mass Transfer 42 (1999) 3739–3756.
[4] M. Almogbel, A. Bejan, Constructal optimisation of nonuniformly distributed tree-shaped flow structures for conduction, Int. J. Heat Mass Transfer 44 (2001) 4185–4194.
[5] A. Bejan, Constructal-theory networks of conducting paths for cooling a heat generating volume, Int. J. Heat Mass Transfer 40 (1997) 799–816.
[6] J. Dirker, A.G. Malan, J.P. Meyer, Numerical modelling and characterisation of the thermal behaviour of embedded rectangular cooling inserts in modern heat generating mediums, in: Proceedings of the 3rd International Conference on Heat Transfer, Fluid Mechanics, and Thermodynamics (HEFAT 2004), Cape Town, South Africa, 21–24 June 2004, Paper No. DJ1.
[7] J. Dirker, W. Liu, J.D. Van Wyk, J.P. Meyer, Evaluation of embedded heat extraction for high power density integrated electromagnetic power passives, in: Proceedings of the Power Electronics Specialist Conference (PESC), 21–25 June, 2004, Paper No. 11430.
[8] J. Dirker, W. Liu, J.D. Van Wyk, A.G. Malan, J.P. Meyer, Embedded solid state heat extraction in integrated power electronic modules, IEEE Trans. Power Electron. 20 (3) (2005) 694–703.
[9] L. Gosselin, A. Bejan, Constructal thermal optimisation of an electromagnet, Int. J. Therm. Stresses 43 (2004) 331–338.
[10] L.-T. Yeh, R. Chu, Thermal Management of Microelectronic equipment: Heat Transfer Theory, Analysis Methods and Design Practices, ASME Press, 2002.
[11] J. Dirker, A.G. Malan, J.P. Meyer, Thermal characterisation of rectangular cooling shapes in solids, Int. J. Numer. Meth. Heat Fluid Flow 17 (2007) 361–383.
[12] C.-E. Fröberg, Numerical Mathematics: Theory and Computer Applications, The Benjamin/Cummings Publishing Company, Inc., 1985.